Improving the quality of continuous ultrasonically welded thermoplastic composite joints by adding a consolidator to the welding setup

Jongbloed, B.C.P.; Vinod, R.; Teuwen, Julie J.E.; Benedictus, R.; Villegas, I.F.

DOI
10.1016/j.compositesa.2022.106808

Publication date
2022

Document Version
Final published version

Published in
Composites Part A: Applied Science and Manufacturing

Composites: Part A 155 (2022) 106808

Contents lists available at ScienceDirect

Composites Part A

journal homepage: www.elsevier.com/locate/compositesa

Improving the quality of continuous ultrasonically welded thermoplastic composite joints by adding a consolidator to the welding setup

Bram Jongbloed *, Rahul Vinod, Julie Teuwen, Rinze Benedictus, Irene Fernandez Villegas

Department of Aerospace Structures and Materials, Faculty of Aerospace Engineering, Delft University of Technology, Kluyverweg 1, 2629 HS Delft, the Netherlands

ARTICLE INFO

Keywords:
Fusion bonding
Ultrasonic welding
Consolidation
Joining
CF/PPS

ABSTRACT

Continuous ultrasonic welding is a promising high-speed and energy-efficient joining technique for thermoplastic composite structures. However, in the current state-of-the-art research on the topic numerous deconsolidation voids could be identified at the welding interface, which results in a strength knock-down. The aim of this study is, therefore, to improve the quality of continuous ultrasonically welded joints by adding a consolidation shoe to the welding setup. To determine the required consolidation pressure, the size of the shoe, and its distance from the sonotrode a stepwise approach was followed based on the static ultrasonic welding process. The closest consolidation distance, best representing the static welding conditions, did not improve the weld quality as significant porosity was still found in the weld line and in the adherends. However, for the furthest consolidation distance high-quality continuous welds were obtained with almost no porosity and a high strength.

1. Introduction

The interest and the application of thermoplastic composites is increasing in the aerospace industry due to their advantages over the currently more common thermoset composites. The main advantages are that thermoplastics can be re-molten and reshaped upon heating, they are recyclable, and have a high material toughness. Especially, the first advantage can lead to major cost benefits, since it makes efficient forming and welding techniques possible. As a result, different welding techniques have been developed for joining thermoplastic composite structures. The most promising welding techniques are resistance, induction, and ultrasonic welding [1]. Ultrasonic welding is currently the least developed of the three. It however stands out because of its high heat generation rates, as demonstrated by the comparative evaluation of the heating times necessary to produce welds of a certain size [2,3], and hence because of its potential to enable high-speed industrialized welding processes.

The ultrasonic welding process consists of a heating phase, known as vibration phase, during which the thermoplastic resin softens and melts, and a consolidation phase during which the weld cools down and solidifies. Heat is generated as follows: a metal horn, called a sonotrode, transversely exerts high-frequency low-amplitude vibrations to the weld interface, while at the same time applying a static pressure. Heat is generated at the weld interface due to surface and viscoelastic friction [4,5]. To focus heat generation at the interface, an energy director is used [6]. This energy director is a layer of resin, i.e. a resin film or a mesh woven from thermoplastic resin filaments. Due to its lower stiffness and subsequent higher cyclic straining under the imposed vibrations, the viscoelastic heating undergone by the energy director is higher compared to that undergone by the fibre reinforced adherends [7–9].

Fig. 1. Cross-sectional view of the mesh energy director adapted from [10].

Two ultrasonic welding processes can be distinguished, static (i.e. spot) and continuous welding [6]. During static welding both the sonotrode and adherends remain stationary during the welding process (which can be sequentially performed at different locations), while for the continuous process the sonotrode and the adherends move relative to each other during the welding process creating a continuous

* Corresponding author.
E-mail address: B.C.P.Jongbloed@tudelft.nl (B. Jongbloed).

https://doi.org/10.1016/j.compositesa.2022.106808
Received 31 August 2021; Received in revised form 9 December 2021; Accepted 3 January 2022
Available online 15 January 2022

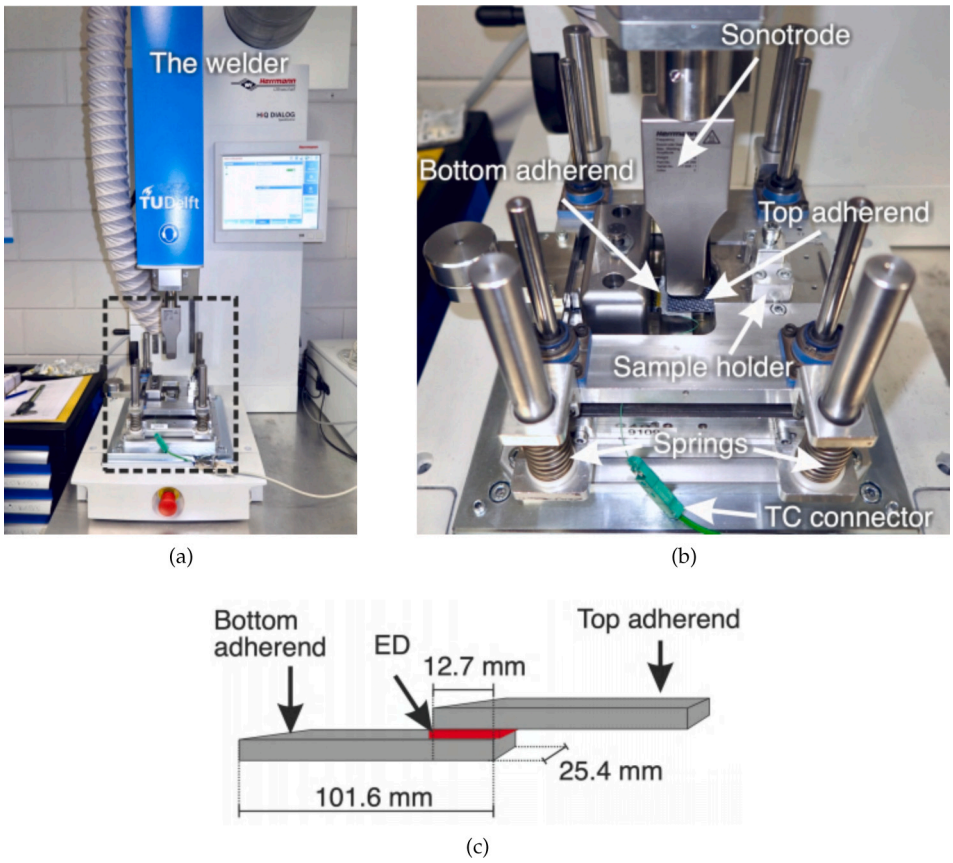

Fig. 2. (a) Ultrasonic welder from Herrmann Ultrasonics. (b) Custom-built welding fixture with spring resting sample holder for top adherend. (c) Schematic of adherends and energy director (ED) in static process.

welded seam. The continuous ultrasonic welding process potentially has benefits over the static counterpart for certain applications. A generally larger welded area means a higher load carrying capability for the continuously welded joints. Continuous ultrasonic welding of thermoplastic composites is however a relatively new technology that still requires optimization. One of the important aspects to be optimized is the quality of the continuous welded joints [10–12]. Indeed, in a previous study [12] in which we compared the static and continuous ultrasonic welding processes for different welding parameters, we found a significantly lower maximum strength for the continuous welded joints. The lower strength was attributed to the presence of voids due to a lack of consolidation during cooling down. In the static process, the sonotrode itself provides the consolidation pressure during cooling. In the continuous process, on the other hand, the sonotrode cannot apply the consolidation pressure, because it continuously moves away from the area that was just heated up [12]. Up to now, most studies on ultrasonic welding of thermoplastic composites have focused on the vibration or heating phase of the static welding process [6,8,13–22], but not on the consolidation or cooling phase. Nevertheless, the consolidation is at least as important since it majorly impacts the void content, the autohesion process and ultimately the strength of the joint. Deconsolidation is a potential problem that can occur when processing thermoplastic composites and which significantly increases the void content reducing the quality of the material [23,24]. It can occur when insufficient consolidation pressure is applied [25–27] or when the pressure is not applied for a long enough time during cooling. For amorphous matrices deconsolidation can occur when the temperature is sufficiently high above the glass transition temperature and for semi-crystalline matrices above the melting temperature [25,28]. Deconsolidation typically is driven by either one of the following two factors: fibre decompaction due to the release of internal stresses [25–27,29,30] especially for fabrics; and the expansion of already existing voids and moisture [25,26,31].

The aim of this study is to investigate how the quality of continuous ultrasonically welded joints can be improved by adding a consolidation shoe (hereafter referred to as consolidator) to the welding setup. To determine the required consolidation pressure, the size of the consolidator, and its distance from the sonotrode the following steps were followed. Firstly, the effect of consolidation pressure on the weld quality was studied in the static ultrasonic welding process for a constant and sufficiently long consolidation time. Secondly, the effect of the consolidation time on the weld quality was studied on the static welding process by keeping the consolidation pressure constant and by using different consolidation times defined with the assistance of temperature measurements at the welding interface. Finally, those results were used to determine the consolidation pressure and the size of the consolidator in the continuous ultrasonic welding process. The effect of the distance between the consolidator and the sonotrode on the quality of the weld was lastly investigated. The weld quality was assessed through the presence of voids in the weld line and within the adherends, and through the single-lap shear strength and fractographic analysis of the welded joints.

2. Experimental procedures

2.1. Materials

The thermoplastic composite laminates used for the welding experiments in this study were made out of carbon fibre fabric (five harness satin weave) impregnated with polyphenylene sulphide powder (CF/PPS semipreg), CF 0286 127 Tef4 43% from Toray Advanced

Composites, the Netherlands. The laminates were stacked according to a $[0/90]_{3s}$ sequence and subjected to a consolidation process in a hot platen press for 20 min at 320 °C and 1 MPa pressure, which, based on previous experience, results in void-free laminates. The consolidated laminates had a size of 580 mm by 580 mm and a thickness of approximately 1.85 mm. Rectangular adherends measuring 25.4 mm x 101.6 mm and 220 mm x 101.6 mm were cut from the consolidated laminates for the static and continuous welding experiments, respectively. For both adherend sizes the main apparent fibre orientation was in the 101.6 mm direction. A 0.20 mm-thick woven PPS mesh (PPS100, supplied by PVF GmbH, Germany) was used as energy director in all experiments to focus heat generation at the welding interface [10,12]. The mesh, shown in Fig. 1, has a plain weave, an 37% open area, and a mesh count of 39 per cm for both the warp and weft.

2.2. Static ultrasonic welding

The ultrasonic welder (HiQ DIALOG 6200, Herrmann Ultrasonics) shown in Fig. 2(a) was used for all static ultrasonic welding experiments. The operating frequency of the welder is 20 kHz. The welding train consists of a converter, booster and sonotrode. A rectangular sonotrode with a 15 mm x 27 mm contact area was used in these experiments. A custom-built fixture, shown in Fig. 2(b), was used to clamp the adherends in a single-lap configuration (Fig. 2(c)) with an overlap area of 12.7 mm x 25.4 mm. In this fixture, the top adherend is kept in place by a sample holder resting on springs to minimize potential bending of the top adherend as the energy director melts and is squeezed out during the welding process. These springs apply a 18 N upward force (0.056 MPa) on the sample holder once fully pressed down by the sonotrode during the welding process.

For the vibration phase of the static process the following parameters were used: a peak-to-peak vibration amplitude of 80 μm, a welding force amounting to 500 N (1.6 MPa on the welding overlap), and a vertical sonotrode displacement of 0.07 mm defined according to the methodology described in [16,20]. Note that the vertical displacement of the sonotrode was used to indirectly control the duration of the vibration phase and, hence, the onset of the subsequent consolidation phase. The consolidation pressure and consolidation time were varied independently of each other to understand their effect on the weld quality. Firstly, the effect of the consolidation pressure was studied by using different consolidation pressure values, while keeping the consolidation time fixed at 10 s to exclude influences of time on the results. Secondly, the effect of the consolidation time was studied by selecting different consolidation times based on exploratory temperature measurements at the weld interface while keeping the consolidation pressure constant at 1.6 MPa (500 N). An overview of the welding parameters used in this study is shown in Table 1.

2.3. Continuous ultrasonic welding

The custom-built ultrasonic welding machine shown in Fig. 3(a) was used for the continuous ultrasonic welding experiments. It consists of a stiff frame with a X-Y table on a guiding system, an off-the-shelf 20 kHz ultrasonic welder from Herrmann Ultrasonics (VE20 SLIMLINE DIALOG 6200), and a custom-built consolidation unit. Similar to the static ultrasonic welding process, a rectangular sonotrode with a 15 mm x 27 mm contact area was used in the welding setup. The consolidation unit (Fig. 3(b)) consisted of a servo press kit YJKP of 1.5 kN from Festo, a stabilization guide unit to avoid sideways deflections, and a copper block (Fig. 3(c)) in charge of applying the consolidation pressure on the material. The width of the copper block was 30 mm. Copper was chosen to promote heat dissipation away from the overlap as a result of its high thermal conductivity. The length of the copper block as well as the consolidation pressure were defined based on the results from the static tests. The placement of the consolidator with respect to the sonotrode could be changed via the adjustment wheel

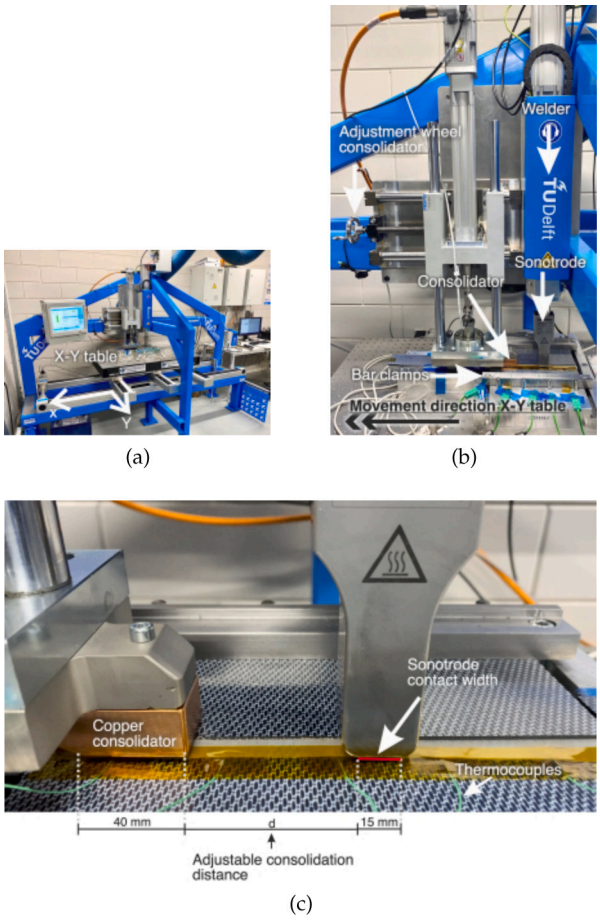

Fig. 3. (a) In house developed continuous ultrasonic welding machine, (b) close-up of the consolidation device and the welder, (c) close-up of consolidator placement.

(Fig. 3(b)). The consolidation distance was defined as the distance between the sonotrode and the consolidator, as indicated in Fig. 3(c). Three consolidation distances were considered in this study: 18.4 mm, 63 mm, and 86.4 mm. Additionally, a continuous weld obtained with the use of no consolidator was produced and used as a reference. An overview of the continuous welds made in this study is shown in Table 1.

During the welding process the X-Y table was translated by an servo motor underneath the sonotrode in X-direction (see Fig. 3(a)). The resulting relative movement of adherends with respect to the sonotrode and consolidator is indicated in Fig. 3(b). The sonotrode was oriented with its 15 mm-wide side parallel to the direction of translation (Fig. 3(c)). A welding force amounting to 500 N (2.6 MPa on the welding overlap), a peak-to-peak amplitude of 80 μm, and a constant welding speed of 35 mm/s were used based on the results of a previous study [12]. Note that the resulting pressure from the 500 N welding force in the continuous process was higher compared to the static process. The top and bottom adherends (Fig. 4(a)) were kept in place by two aluminium bar clamps located at 130 mm from each other (Fig. 4(b)). Note that the configuration used in this study, which we found to provide a more uniform temperature distribution across the overlap (Fig. 5), differs slightly from the one used in our previous study [12] both in distance between bar clamps and in the position of the sonotrode relative to the overlap (Fig. 5). Each clamp was secured with two M8 bolts tightened at a torque of 14 N/m.

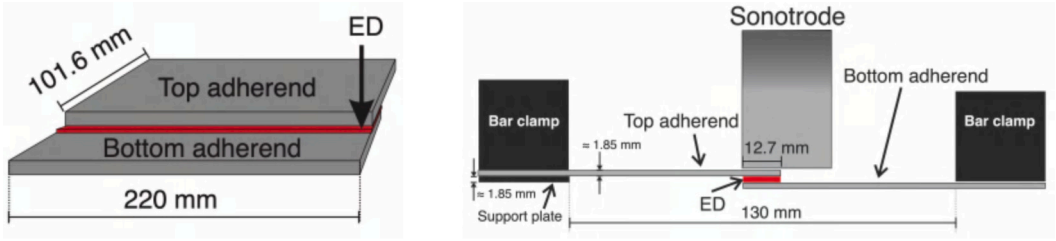

(a) (b)

Fig. 4. Schematic of (a) dimensions of the adherends, and (b) sonotrode and clamps placement for the continuous ultrasonic welding process.

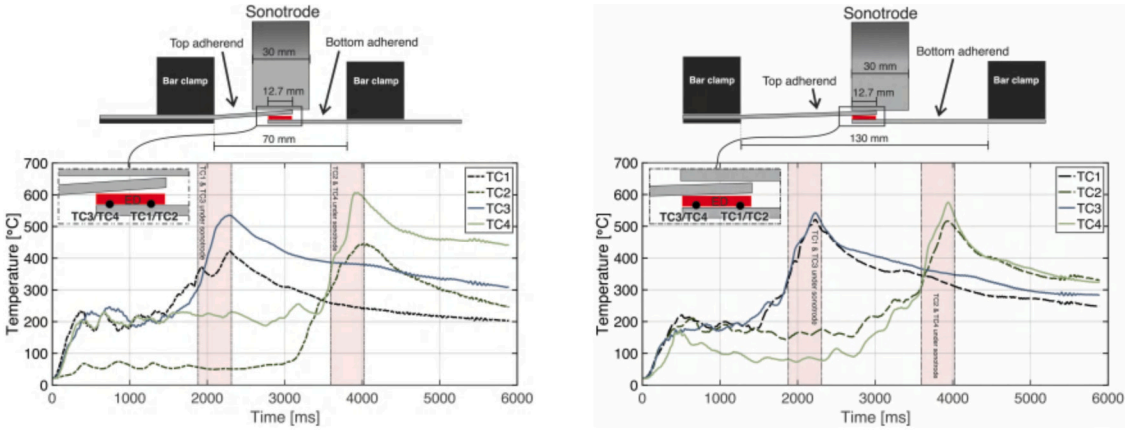

(a) (b)

Fig. 5. Temperature profiles during the continuous welding process for thermocouples placed at the weld interface approximately 2 mm from the edges for (a) 70 mm clamping distance as used in [10,12], and (b) 130 mm as used in the current study as shown in Fig. 4a. The angle between the top adherend and energy director has significantly been over-exaggerated. The red shaded areas indicate when a pair of thermocouples was located under the sonotrode. Welding force was 500 N, vibrational amplitude was 80 μm, welding speed was 35 mm/s, and without consolidator.

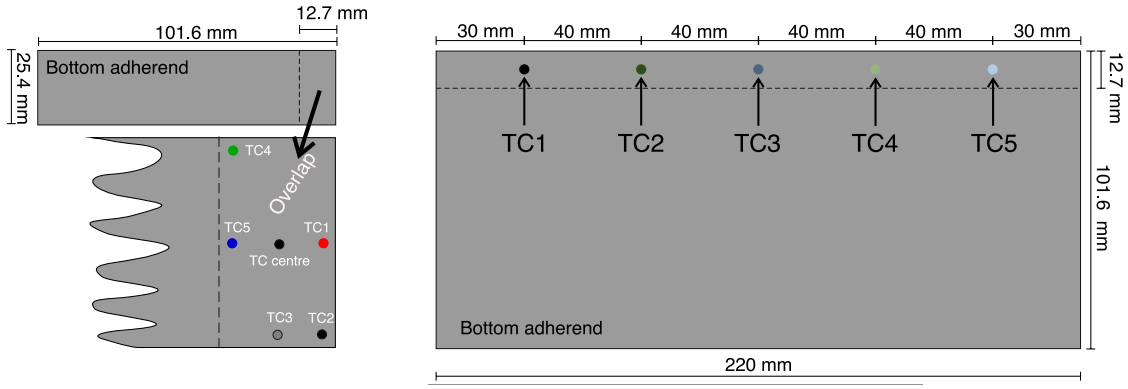

(a) (b)

Fig. 6. Bottom adherends for (a) the static and (b) the continuous ultrasonic welding setup together with the locations where thermocouples (TCs) were placed. The dotted lines indicates the end of the 12.7 mm overlap.

2.4. Temperature measurements

Temperatures were measured at the welding overlap using K-type thermocouples (GG220-2K-0, product number 2-2200-0004, Tempco B.V., Bodegraven, the Netherlands). The sleeved thermocouples had a total diameter of 0.70 mm, while the diameter of the thermocouple wires was 0.10 mm. Note that the sleeve was locally peeled off so that only the naked thermocouple wires were placed at the welding interface. An analog thermocouple output amplifier (Adafruit AD8495) was used to simultaneously sample temperature readings at 1 kHz from a maximum of five thermocouples. A moving average filter (10 points for the static process and 40 points for the continuous process) was applied in MATLAB to filter out high frequency fluctuations from the temperature data. Fig. 6 shows where the thermocouples were placed for (a) the static and (b) the continuous process. Table 1 provides information about which temperature measurements were performed in which experiments.

2.5. Mechanical testing and fractography

The statically welded joints could directly be mechanically tested to obtain their single-lap shear strength (LSS). The continuously welded joints were cut into six 25.4 mm-wide single lap shear samples after discarding approximately 28.8 mm-wide bands of material at both

Table 1
Overview of static (SUW) and continuous (CUW) ultrasonic experiments. (Note that the amplitude values are peak-to-peak.)

Process	Parameters vibration phase (welding pressure (force), amplitude, displacement/ welding speed)	Consolidation pressure (and force)	Consolidation time / consolidator distance	Adherend size [mm]	Remarks
SUW	1.6 MPa (500 N), 80 μm, 0.07 mm	0 MPa (0 N) 0.4 MPa (130 N) 0.6 MPa (200 N) 1.6 MPa (500 N) 3.1 MPa (1000 N) 4.7 MPa (1500 N)	10000 ms	25.4 x 101.6	6 welds per pressure value of which 5 for LSS and 1 for cross-sectional microscopy No temperature measurements.
	1.6 MPa (500 N), 80 μm, 0.07 mm	1.6 MPa (500 N)	10000 ms	25.4 x 101.6	Only temperature measurements: 5 welds with TC2 (Fig. 6(a)); 1 weld with TC1, TC2, TC3, TC4, and TC5; 1 weld with TC centre
	1.6 MPa (500 N), 80 μm, 0.07 mm	1.6 MPa (500 N)	0 ms, 100 ms, 600 ms, 1000 ms 2500 ms, 4000 ms, 5000 ms, 10000 ms	25.4 x 101.6	7 welds per consolidation time of which 5 for LSS, 1 for cross-sectional microscopy, and 1 for micro-CT. Note: no micro-CT performed for 0 ms, 100 ms, and 2500 ms No temperature measurements.
CUW	2.6 MPa (500 N), 80 μm, 35 mm/s	1.6 MPa (800 N)	No consolidator, 18.4 mm, 63 mm, 86.4 mm	220 x 101.6	1 weld per consolidation distance with all TC's shown in Fig. 6(b) and used for LSS.

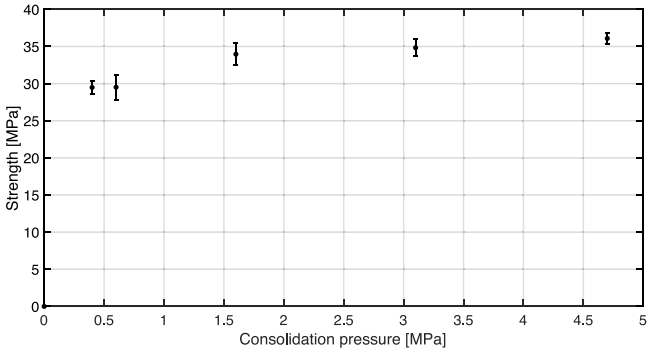

Fig. 7. Average lap shear strength with standard deviation error bars (n=5) for static ultrasonic welds consolidated under different consolidation pressure values.

edges of the joint. Five of these samples were used for mechanical testing, and one sample was used for cross-sectional microscopy. One of the five mechanically tested samples was used for micro-CT prior to mechanical testing. Note that for the static process, samples used for temperature measurements were not used for mechanical testing. However, as shown in Table 1, all the continuously welded plates contained thermocouples at the welding interface according to Fig. 6(b). Therefore, some of the samples for mechanical testing cut from the continuously welded plates contained a thermocouple. The presence of this thermocouple, being very thin, is however not expected to significantly influence the lap shear strength results. The welded single-lap shear samples from both the continuous and static welding processes were mechanically tested using a Zwick/Roell 250 kN universal testing machine under a cross-head speed of 1.3 mm/min. The grips were given the necessary offset to ensure parallelism between the load introduction and the weld line. The LSS was calculated by dividing the maximum load by the overlap area. After mechanical testing, a Keyence VR one-shot 3D (VR-5000) microscope was used to analyse the fracture surfaces.

2.6. Cross-sectional microscopy, and void content determination

To obtain cross-sectional views from the welded adherends, specimens were cut parallel to the longitudinal orientation of the welded samples and embedded in epoxy resin. They were ground and polished with a Struers Tegramin-20 polisher. A Keyence 3D laser scanning confocal (VK-X1000) microscope was used for obtaining the cross-sectional micrographs. A Phoenix Nanotom Micro-CT scanner (180 kV maximum voltage, and 15 W maximum power) was used to quantify the volumetric void content within the welded overlap with a resolution of 14 μm. Avizo CT software from ThermoFisher Scientific was used to determine the volumetric void content based on the total volume of the material in the welded overlap.

3. Results

3.1. Effect of consolidation pressure for the static ultrasonic welding process

Fig. 7 shows the lap shear strength values for static ultrasonic welds consolidated under different consolidation pressure values. The corresponding representative fracture surfaces obtained after mechanical testing are shown in Fig. 8. Representative cross-sectional micrographs are shown in Fig. 9.

3.2. Effect of consolidation time for the static ultrasonic welding process

Fig. 10(a) shows a representative temperature profile of a static ultrasonic weld of both the vibration and consolidation phase. The temperature distribution at the weld interface during the consolidation phase is shown in Fig. 10(b) together with the glass transition temperature (T_g, 97 °C) and the melting temperature (T_m, 280 °C) obtained from a DSC test. Fig. 10(c) shows the temperature profiles measured at the location of TC2 (Fig. 6(a)) for only the consolidation phase of five welds together with the average single-lap shear strength values of welds consolidated for the selected consolidation times. The temperature measured at TC2, being overall the hottest (Fig. 10(c)), was chosen as the representative temperature to ensure that, at a given consolidation time, the temperatures in the entire overlap would be equal or below that value. Note the differences in temperature readings between TC2 and TC4, both located at equidistant corners from the centre, can be attributed to the heat conducted away from TC4 towards the relatively colder material outside of the overlap since the thermocouples were placed in direct contact with the bottom adherend. Hence cooling is faster at TC4 compared to TC2, which on the other

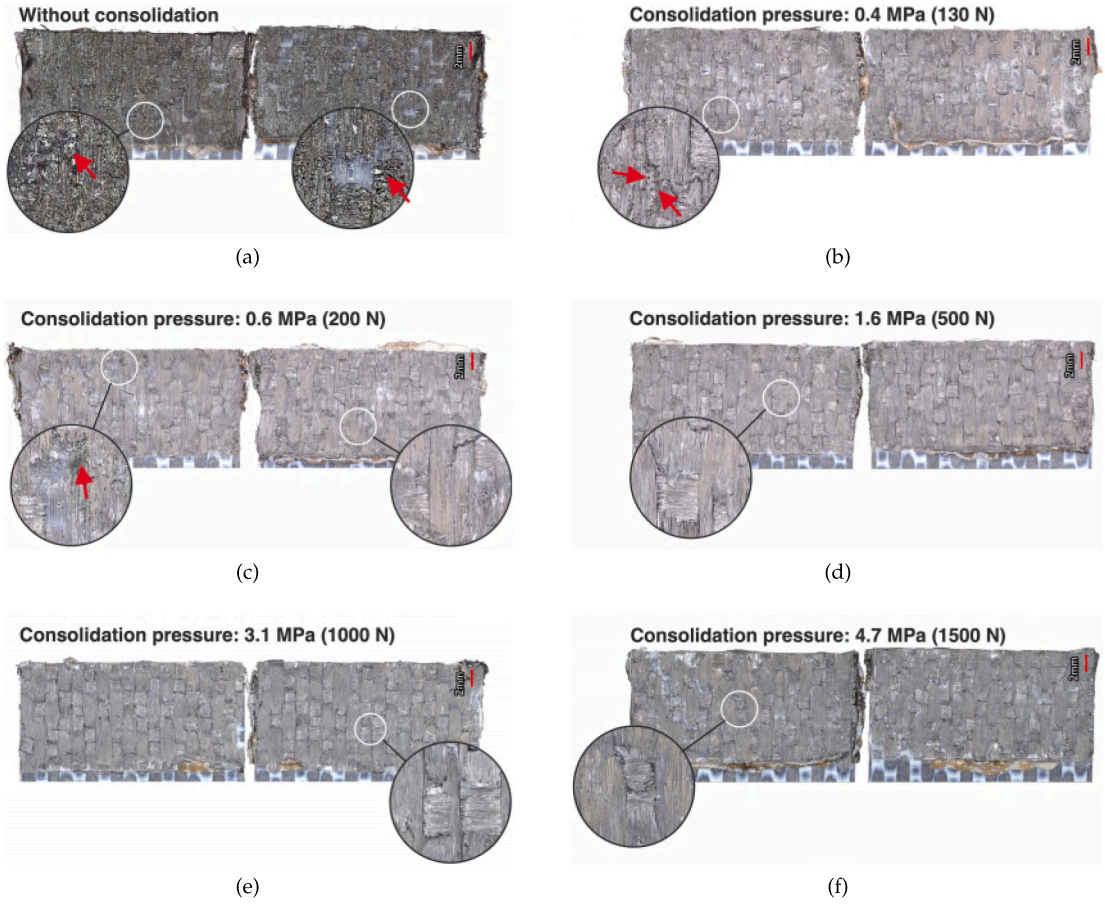

Fig. 8. Representative fracture surfaces of static ultrasonic welds consolidated under different pressure values. The top adherends are shown left, and the bottom adherends are shown right. Some white circled areas are enlarged to show representative details of the fracture surfaces. The red arrows indicate areas containing voids.

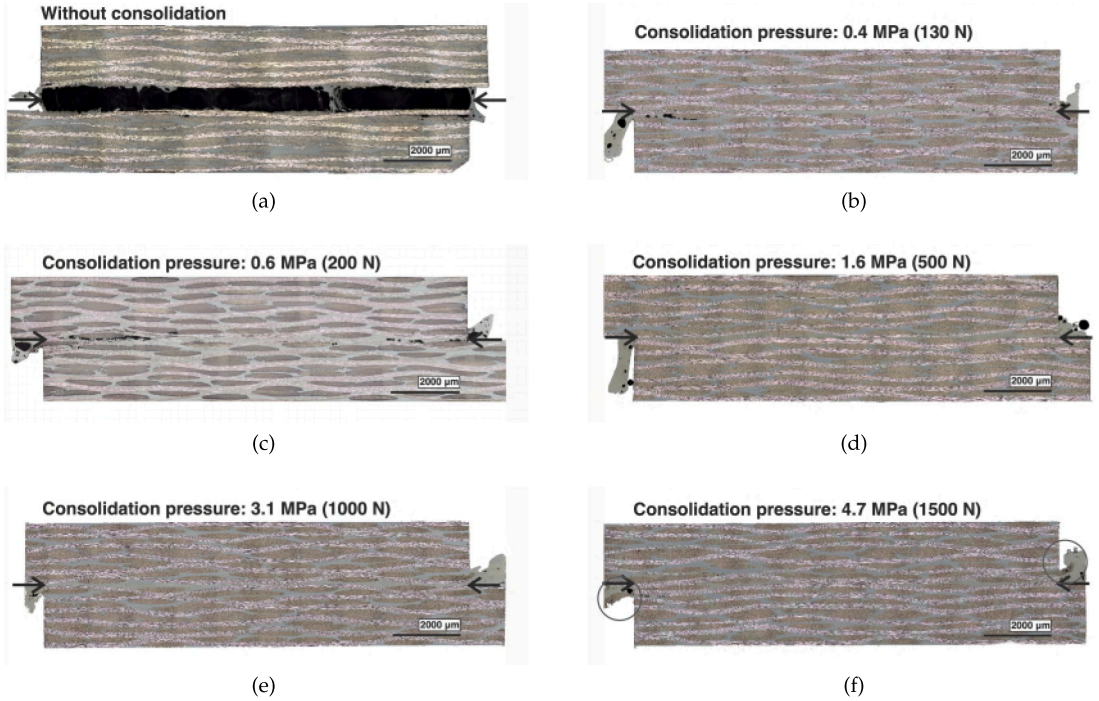

Fig. 9. Representative cross-sectional micrographs of static ultrasonic welds consolidated under different pressures. The black arrows indicate the weld lines. The grey circled areas indicate fibre squeeze-out. The black coloured zone in (a) indicated by the arrows contains air.

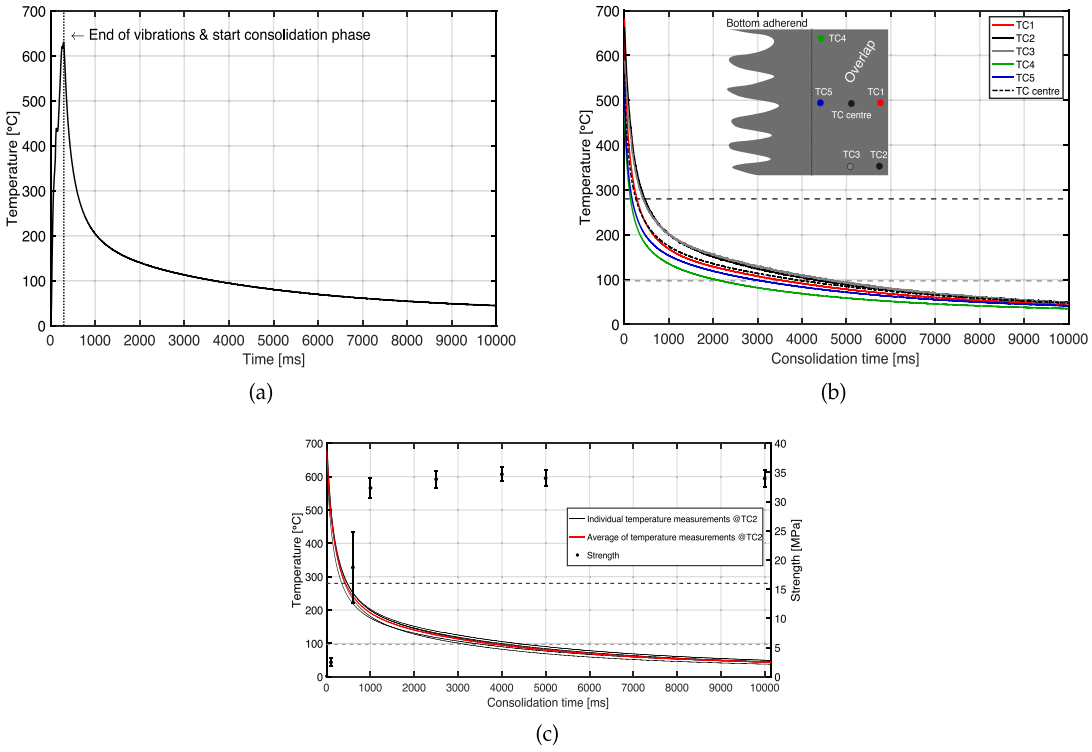

Fig. 10. Temperature profile(s) for the static welding process for (a) both the vibration and the consolidation phase at TC2 location (Fig. 6(a)), and only the consolidation phase (b) at multiple TC locations obtained from 2 welds and (c) at TC2 location for five welds together with their average temperature. Additionally in (c), average lap shear strength values with standard deviation error bars (n=5) are shown for welds consolidated for different consolidation times.

Table 2
Selected consolidation times, corresponding average interface temperature with standard deviation from Fig. 10(c) (n = 5) (rounded to nearest integer 5), corresponding single lap shear strength (LSS) with standard deviation shown (n = 5), and volumetric void content from static welds.

Consolidation time [ms]	Temperature [°C]	Explanation	LSS [MPa]	Void content [%]
0	680 ± 45	No consolidation	0.0	NA
100	485 ± 25	Interface above T_m	2.5 ± 0.7	NA
600	240 ± 15	Interface just below T_m	18.7 ± 6.0	0.61
1000	190 ± 10	Interface in the middle of T_m and T_g	32.3 ± 1.7	0.05
2500	125 ± 10	Interface just above T_g	33.9 ± 1.5	NA
4000	95 ± 10	Interface approximately at T_g	34.7 ± 1.2	0.05
5000	80 ± 10	Interface just below T_g	34 ± 1.4	0.07
10000	45 ± 5	Interface well below T_g	34 ± 1.5	0.06

hand is close to the free edge of the adherend and practically thermally insulated by the surrounding air. Table 2 summarizes the interface temperature until which the welds were consolidated, the average single-lap strength, and when available the volumetric void content for the selected consolidation times. Fig. 11 and Fig. 12 shows corresponding representative fracture surfaces and cross-sectional micrographs, respectively, of the welds obtained at different consolidation times.

3.3. Consolidation in continuous ultrasonic welding

Fig. 13 shows the interface temperatures measured at five locations in the overlap during the continuous welding process without the use of the consolidator. The red shaded areas indicate the time span during which a specific thermocouple was located under the sonotrode. The moment the sonotrode completely passed a specific thermocouple was defined as the start of the consolidation phase for that specific thermocouple location. Fig. 14 shows the superimposed temperature profiles of the consolidation phase for the continuous ultrasonic welding process (Fig. 14(a)) without consolidator and (Figs. 14(b), 14(c) and 14(d)) for consolidation distances 18.4 mm, 63 mm and 86.4 mm, respectively. The grey shaded area indicates the time span during which the consolidator applied the consolidation pressure. The obtained strength and the volumetric void content for these four cases is shown in Table 3 and representative fracture surfaces and cross-sectional micrographs are shown in Fig. 15 and Fig. 16, respectively.

Table 3
Average lap shear strength (LSS) with the standard deviation (SD) (n = 5), and volumetric void content of continuous welds for different consolidation distances.

Consolidation distance [mm]	LSS [MPa]	Void content [%]
No consolidator	15.1 ± 2.6	7.80
18.4 mm	9.5 ± 2.9	8.32
63.0 mm	38.6 ± 2.7	N/A
86.4 mm	39.6 ± 2.3	1.01

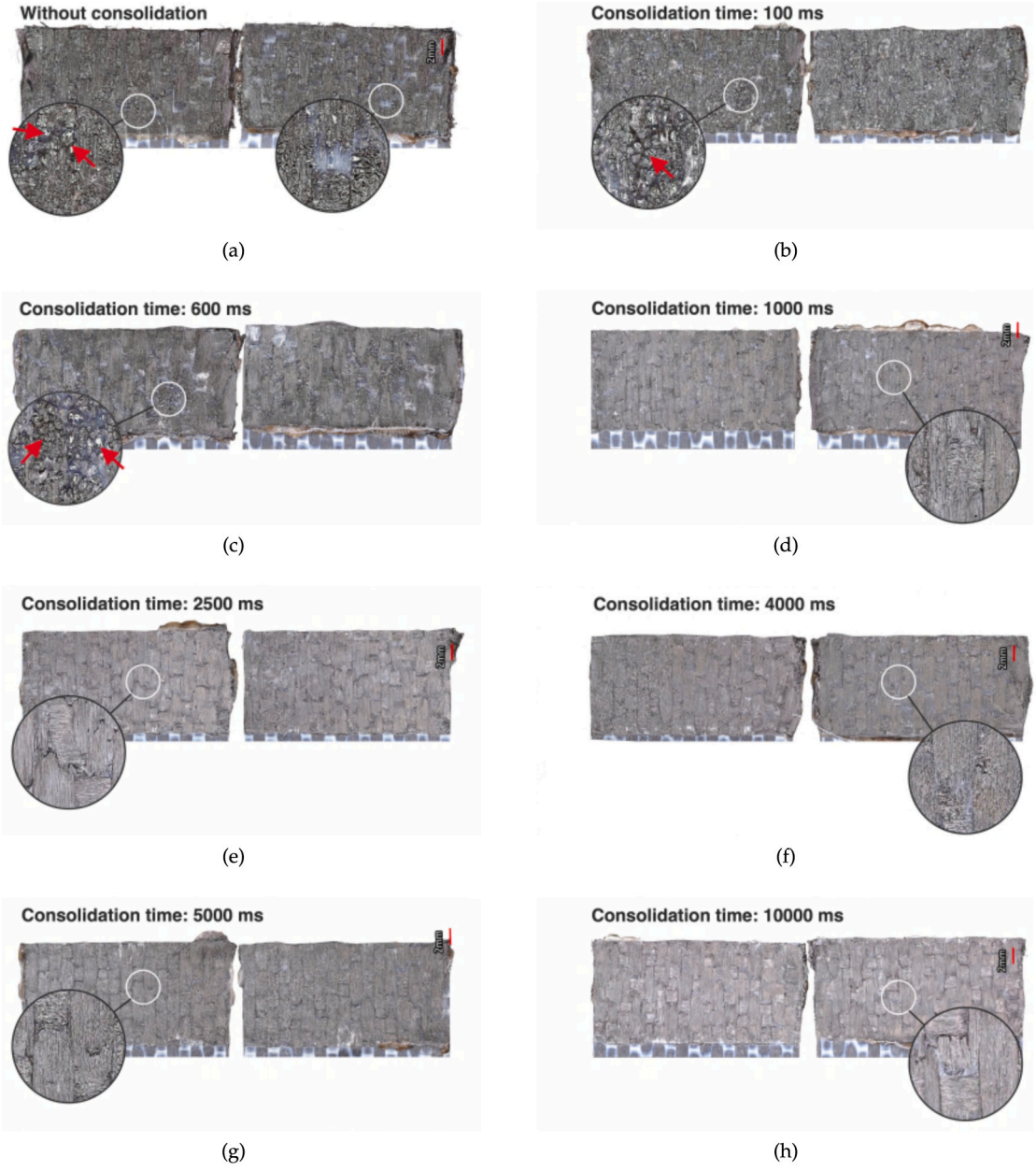

Fig. 11. Fracture surfaces of mechanically tested static ultrasonic welds consolidated for different consolidation times. The top adherends is shown left, and the bottom adherends is shown right. The white circled areas are enlarged to show details of the fracture surfaces. The red arrows indicate areas containing voids.

4. Discussion

Low consolidation pressure values (0.4 MPa and 0.6 MPa) during the static welding process resulted in the presence of voids at the weld line as observed on the fracture surfaces (Figs. 8(b) and 8(c)) and cross sections (Figs. 9(b) and 9(c)). The pressure was most likely not sufficient to eliminate the initial air present within the open areas of the energy director. The resulting voids contributed to the observed reduction in strength at low consolidation pressures (Fig. 7). For the higher consolidation pressure values (1.6 MPa, 3.1 MPa, and 4.7 MPa), on the other hand, the pressure was sufficient to minimize the number of voids (Figs. 8(d), 8(e), 8(f), 9(d), 9(e), and 9(f)). Consequently, a higher strength, similar for all these high consolidation pressure values (Fig. 7), was obtained.

For consolidation times of 1000 ms or longer in the static process a similar high weld quality was obtained in terms of practical absence of voids (Figs. 11(d) to 11(h), 12(d) to 12(h), and Table 2) and high strength (Fig. 10(c)). Regarding the temperature evolution within the welding overlap (Fig. 10(b)), at 1000 ms consolidation time the temperature was found to be within 200 °C and 135 °C, with the highest temperatures measured at the longitudinal edge, TC2 location. Temperatures at all locations were found to drop below Tg of the PPS resin only after 5000 ms consolidation time.

It is interesting to note that the maximum rate of crystallization of PPS falls within the temperature range measured at 1000 ms consolidation time. Indeed, Chung and Cebe [32] and Furushima et al. [33] reported it to be between 170 °C to 190 °C and at 160 °C, respectively. Consequently, the crystallization of the polymer in the weld line is believed to play an important role in the development of weld strength during consolidation. Extra DSC experiments were conducted on polymer material extracted from the weld line by sandwiching the energy director in between two kapton films during the welding process, as described by Koutras et al. [21]. This resulted in a degree of crystallinity of 10.7 ±1.0% (n=3) when the weld was consolidated for

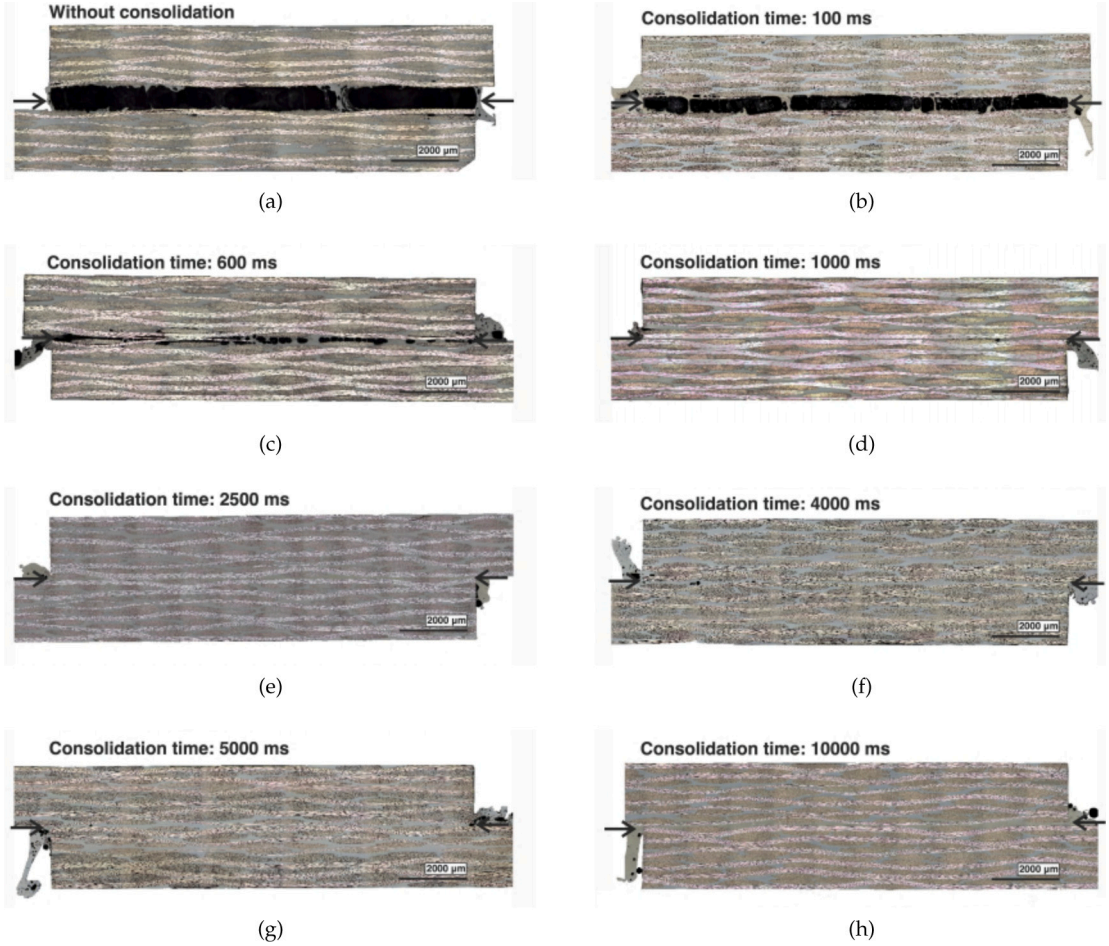

Fig. 12. Cross-sectional micrographs of static ultrasonic welds consolidated for different consolidation times. The black arrows indicate the weld line. The black coloured zones in (a,b, and c) in between the arrows consist of air.

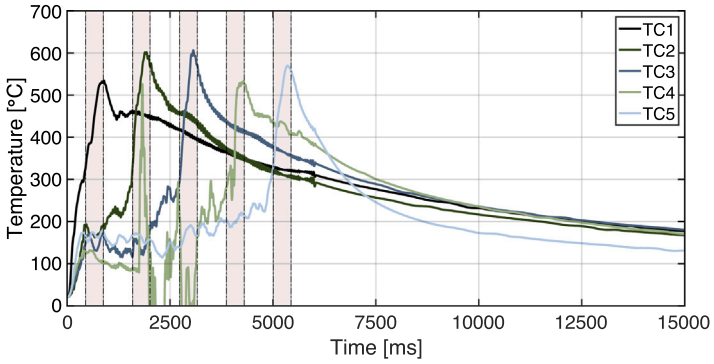

Fig. 13. Temperature profiles measured by five thermocouples (TC) placed according to Fig. 6b of a continuous ultrasonic weld without the use of a consolidator. The shaded areas indicate when a particular thermocouple was located under the sonotrode during the welding process.

1000 ms, which proves that crystallization occurs in ultrasonic welding despite the high cooling rates. For these extra experiments a Perkin Elmer DSC 8500 was used and the degree of crystallinity was calculated using the following equation:

$$X_c = \frac{\Delta H_m - \Delta H_c}{\Delta H_f^o} \cdot 100[\%],$$

in which ΔH_m [J/g] is the measured specific melting enthalpy, ΔH_c [J/g] is the measured specific energy from cold crystallization [J/g], and $\Delta H_f^o = 112$ [J/g] [34] is the specific melting enthalpy of an ideal crystal.

Based on the minimum consolidation pressure and time necessary for high weld quality in the static welding process, the consolidation pressure and length of the consolidator in the continuous process were set at 1.6 MPa and 40 mm, respectively, which corresponds to approximately 1100 ms of consolidation at a welding speed of 35 mm/s. High-quality continuously welded joints with virtually no porosity, low void content, and high strength were obtained under such consolidation conditions and the longest distance (86.4 mm) between consolidator and sonotrode (Fig. 16(d) and Table 3), however some fundamental differences with the static process could be identified. Firstly, the cooling rates were overall lower and hence the temperatures

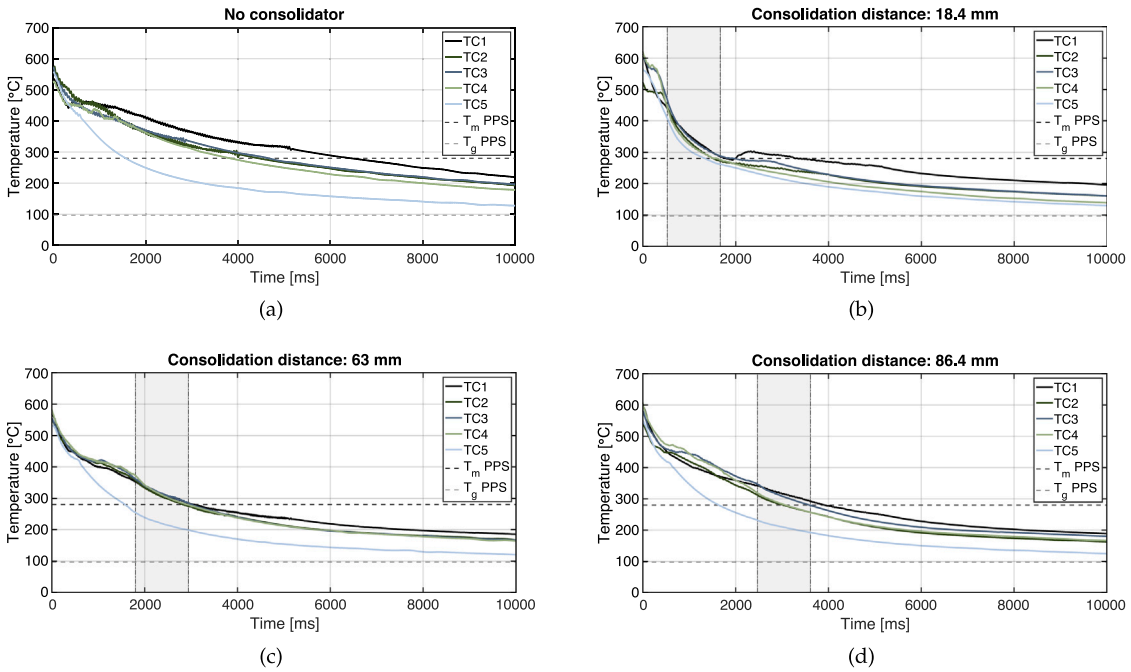

Fig. 14. Superimposed temperature profiles of the consolidation phase of continuous ultrasonic welds displayed for each thermocouple from the moment the sonotrode passed the individual thermocouple for different consolidation cases: (a) no consolidator, (b, c, and d) with consolidator at a consolidation distance of 18.4 mm, 63.0 mm and 86.4 mm respectively. The grey shaded area indicates the time span during which the consolidator applied the consolidation pressure.

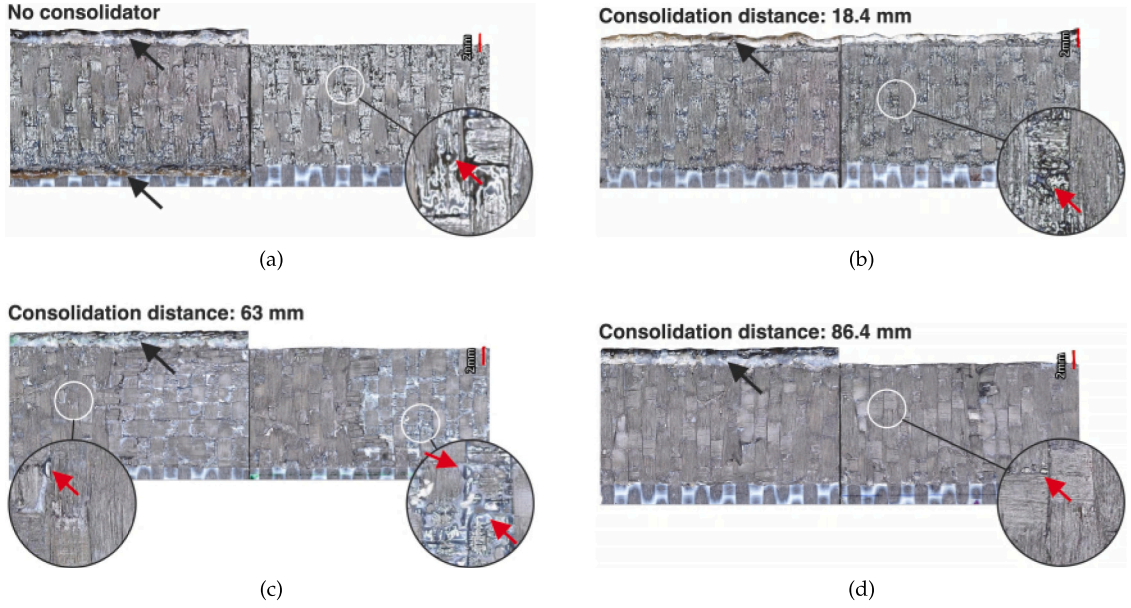

Fig. 15. Representative fracture surfaces of mechanically tested samples of continuous ultrasonic welds consolidated: (a) without consolidator, and (b, c, and d) for consolidation distances of 18.4 mm, 63 mm and 86.4 mm, respectively. The left samples show the top adherends, and right samples show the bottom adherend. White circled areas are enlarged to show details of the fracture surfaces. The black arrows indicate excessive fibre and resin squeeze out. The red arrows indicate areas with voids.

measured at the welding interface just behind the consolidator were around 280 °C for all three considered consolidator-sonotrode distances (Fig. 14). These were well above the 200 °C-135 °C critical temperature range defined by the static process. The fact that continuous welds with virtually no porosity could be obtained despite the high interface temperatures may be related to the compressive force applied on the welding interface by the clamping jig in the continuous process as opposed to the tensile force caused by the clamping jig in the static process. Secondly, the shortest consolidator-sonotrode distance in the continuous welding process, which among all the cases studied is the one that best approximates the consolidation conditions during the static process, resulted however in the lowest overall weld quality (Fig. 16(b) and Table 3). Analysis of the state of the material in the area between sonotrode and consolidator with only some voids present (see II in Fig. 17) suggests that, in that case, the observed porosity (see I in Fig. 17) and subsequently lower strength was potentially caused by the passing of the consolidator. In particular, based on qualitative analysis of the squeeze-out in the cross-sectional micrographs in Figure 16, the pressure applied by the consolidator might have caused significant matrix squeeze-out from the welding interface and the areas of the adherends adjacent to the welding interface, which locally reduces the resin volume fraction, therefore resulting in a relatively drier fibre bed

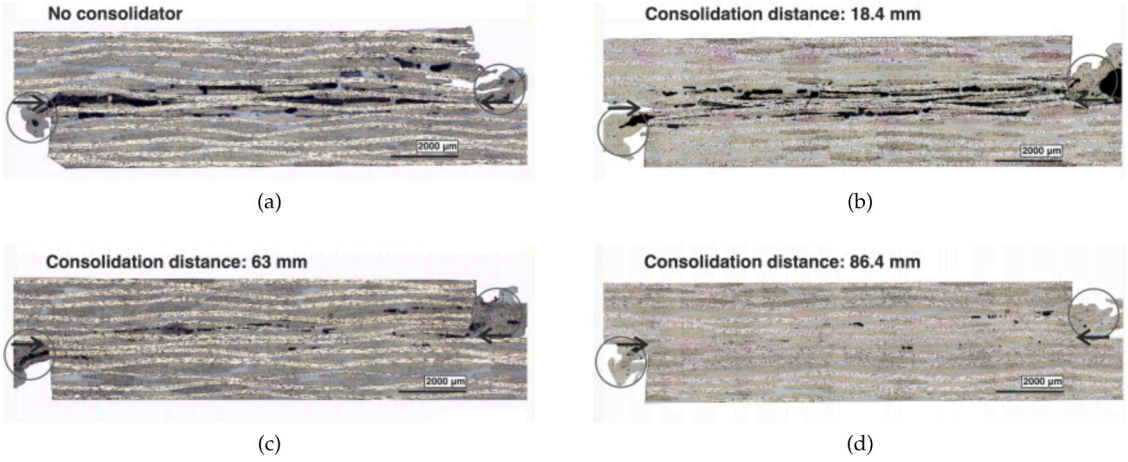

Fig. 16. Representative cross-sectional micrographs of continuous ultrasonic welds consolidated: (a) without consolidator, and (b, c, and d) for consolidation distances of 18.4 mm, 63 mm and 86.4 mm, respectively. The black arrows indicate the weld line. The grey circles indicate fibre and resin squeeze-out.

at/around the interface. Upon removal of the consolidation pressure (i.e. the passing of the consolidator), porosity (Figure 16(b)) can then be observed caused by spring back of the relatively dry fibre bed. Based on the same qualitative analysis of the cross-sections in Figure 16, significant squeeze-out was also observed when the consolidator was located further away from the sonotrode (Figures 16(c) and 16(d)). This, however, caused little (Figure 16(c)) to no porosity (Figure 16(d)) most likely because in those cases the fibres were locally squeezed out together with the matrix. Consequently, the resin volume fraction was not as significantly reduced as in the previous case. The difference in flow type, predominantly matrix (for closest consolidation distance) versus matrix and fibres (for further consolidation distances), is likely caused by a difference in viscosity [35] due to the potential temperature differences of the matrix under the consolidator. However, a more comprehensive analysis of the composition of the squeeze-out of the adherends would be needed as solid evidence to support this hypothesis.

Another factor that likely contributes to the observed porosity for the closest (18.4 mm) consolidation distance is deconsolidation. The thermal history in the adherends might be different for the three consolidation distances, despite the similar interface temperatures after passing of the consolidator (Figure 14), which can lead to different degrees of deconsolidation. Consequently, the highest degree of deconsolidation would be expected at the closest consolidation distance due to insufficient cooling of the matrix under the consolidator to allow for solidification under pressure. This results in porosity after passing of the consolidator. Then, for the welds made with the furthest consolidation distance (86.4 mm), the matrix most likely solidified sufficiently to allow consolidation under pressure. Unfortunately, our attempts to prove this hypothesis by measuring the temperature within the top adherend (the one with the highest degree of porosity, see Figure 16) were unfruitful owing to severe overheating caused by the ultrasonic vibration at the location of the thermocouples.

It is interesting to note that none of the static welds investigated in this work displayed the severe porosity in the adherends observed in Figs. 16(a) and 16(b), which suggests that the continuous ultrasonic welding process causes more bulk heating in the adherends than the static process. The significantly slower cooling measured at the welding interface in the continuous process is also consistent with such hypothesis (less efficient heat transfer owing to warmer surroundings). The higher welding pressure used for the continuous process (see Table 1) could have caused faster heat generation in the adherends and, by that, contributed to the observed bulk heating. However, further research is necessary to understand which factors have an effect on the difference in bulk heating observed between the two processes. In any case, such fundamental difference indicates that the process followed in the present paper to determine the size and position of the consolidator (i.e., direct translation from the static to the continuous process) is only a first approximation and needs to be refined (as it is clear from the results obtained from the shortest consolidation distance). Additionally, the promising results obtained with the longest consolidation distances indicate that, once the consolidation pressure has been defined, the effectiveness of the consolidator is defined by at least two parameters, i.e., its size and position with regards to the sonotrode. This is a positive result since it adds an extra degree of flexibility to the continuous process with regards to the static one, with only one parameter, i.e. consolidation time, to determine the effectiveness of the consolidation phase.

The strength values measured in the continuous welded joints in the cases in which the consolidator was located 63 mm and 86.4 mm away from the sonotrode were even higher than the strength values measured in the static welded joints. We believe this difference is mostly caused by the reduction of peel stresses at the edges because of both the taper and fillet associated with the matrix and fibre squeeze-out (Figs. 16(c) and 16(d)). Potential differences in weld line thickness related to the squeeze out of the energy director may play a role as well. It should be noted that the strength measured in the continuous welds obtained in the absence of consolidator (Table 3) was significantly lower than that reported in our previous studies [10,12]. This difference is attributed to the differences in clamping distance (130 mm vs. 70 mm in previous studies) and the indirect pressure applied by the clamps on the welded overlap.

5. Conclusions

The aim of this study was to improve the quality of continuous ultrasonically welded joints by adding a consolidator to the welding setup. To determine the required consolidation pressure, the size of the consolidator, and its distance from the sonotrode a stepwise approach was taken based on the static process. Firstly, the effect of the consolidation pressure on the quality of welds obtained through a static ultrasonic welding process was studied. Low consolidation pressure values (0.4 MPa and 0.6 MPa) resulted in voids and a reduced strength. For pressure values of 1.6 MPa and above a similar high weld quality in terms of reduced presence of voids and strength increase was observed. Secondly, the effect of the consolidation time on the quality of static welds was studied. For consolidation times of 1000 ms or longer a similar high weld quality was observed, which is believed to be related crystallization of the polymer in the weld line. Finally, based on the minimum consolidation pressure and time necessary for high weld quality in the static welding process, the consolidation pressure and length of the consolidator in the continuous process were set at 1.6

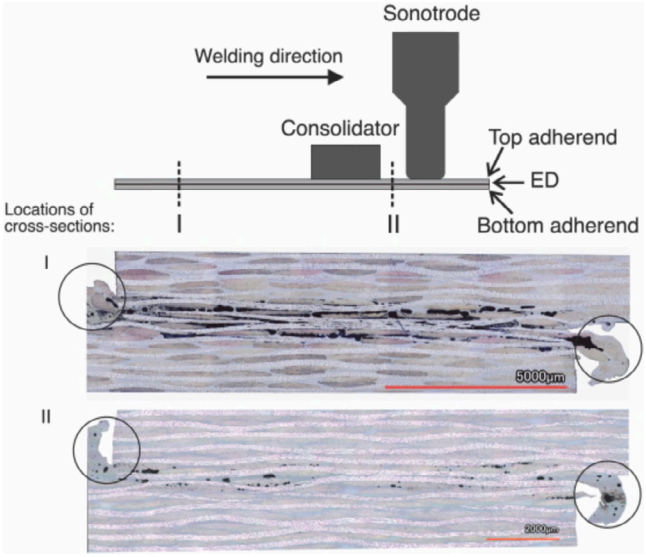

Fig. 17. Schematic of sonotrode and consolidator placed 18.4 mm from the sonotrode together with indicated locations from where cross-sectional micrographs were taken after the process was stopped in the shown position: after consolidator passed (I) (taken from Fig. 16b), and in between the sonotrode and consolidator (II). The consolidator was kept on the overlap for 60 s after stopping the welding process.

MPa and 40 mm, respectively. High-quality continuously welded joints with virtually no porosity and high strength were obtained under such consolidation conditions and the longest distance between consolidator and sonotrode. The closest consolidation distance, best representing the static welding conditions, did not improve the weld quality as porosity was still observed in the weld line and in the adherends. Such apparent contradiction is however consistent with more bulk heating generated in the adherends in the continuous process, as clearly evidenced by the results in this paper. The reasons for such different behaviour are currently unknown and should be investigated in further research.

CRediT authorship contribution statement

Bram Jongbloed: Conceptualization, Methodology, Investigation, Formal analysis, Writing – original draft, Writing – review & editing, Visualization. **Rahul Vinod:** Methodology, Investigation, Formal analysis, Visualization. **Julie Teuwen:** Conceptualization, Methodology, Supervision, Writing – review & editing. **Rinze Benedictus:** Resources, Supervision. **Irene Fernandez Villegas:** Conceptualization, Methodology, Resources, Writing – review & editing, Supervision, Project administration, Funding acquisition.

Declaration of competing interest

The authors declare that they have no known competing financial interests or personal relationships that could have appeared to influence the work reported in this paper.

Acknowledgements

This study was funded by the European research programme Clean Sky. The ecoTECH project has received funding from the European Union's Horizon 2020 Clean Sky 2 Joint Undertaking under the AIRFRAME ITD grant agreement number GAM AIR 2020 – 945521. The authors would like to especially thank Rein van den Oever, Perry Posthoorn, and Jan Graafland from the Electronic and Mechanical Support Division from the TUDelft for the electronic and software development of the consolidator for the continuous ultrasonic welding machine.

References

[1] Ageorges C, Ye L, Hou M. Advances in fusion bonding techniques for joining thermoplastic matrix composites: A review. Composites A 2001;32(6):839–57.
[2] Villegas IF, Moser L, Yousefpour A, Mitschang P, Bersee HE. Process and performance evaluation of ultrasonic, induction and resistance welding of advanced thermoplastic composites. J Thermoplast Compos Mater 2013;26(8):1007–24.
[3] Reis JP, de Moura M, Samborski S. Thermoplastic composites and their promising applications in joining and repair composites structures: A review. Materials 2020;13(24).
[4] Potente H. Ultrasonic welding - principles & theory. Mater Des 1984;5(5):228–34.
[5] Zhang Z, Wang X, Luo Y, Zhang Z, Wang L. Study on heating process of ultrasonic welding for thermoplastics. J Thermoplast Compos Mater 2010;23(5):647–64.
[6] Villegas IF. Ultrasonic welding of thermoplastic composites. Front Mater 2019;6:291.
[7] Benatar A, Eswaran RV, Nayar SK. Ultrasonic welding of thermoplastics in the near-field. Polym Eng Sci 1989;29(23):1689–98.
[8] Levy A, Le Corre S, Villegas I. Modeling of the heating phenomena in ultrasonic welding of thermoplastic composites with flat energy directors. J Mater Process Technol 2014;214(7):1361–71.
[9] Grewell D, Benatar A, Park J. Plastics and composites welding handbook, no. 10. Hanser Gardener; 2003.
[10] Jongbloed B, Teuwen J, Palardy G, Villegas IF, Benedictus R. Continuous ultrasonic welding of thermoplastic composites: Enhancing the weld uniformity by changing the energy director. J Compos Mater 2020;54(15):2023–35.
[11] Senders F, van Beurden M, Palardy G, Villegas I. Zero-flow: A novel approach to continuous ultrasonic welding of CF/PPS thermoplastic composite plates. Adv Manuf: Polym Compos Sci 2016;0340(September 2017):1–10.
[12] Jongbloed B, Teuwen J, Benedictus R, Villegas IF. On differences and similarities between static and continuous ultrasonic welding of thermoplastic composites. Composites B 2020;203:108466.
[13] Villegas I. In situ monitoring of ultrasonic welding of thermoplastic composites through power and displacement data. J Thermoplast Compos Mater 2015;28(1):66–85.
[14] Palardy G, Villegas I. On the effect of flat energy directors thickness on heat generation during ultrasonic welding of thermoplastic composites. Compos Interfaces 2017;24(2):203–14.
[15] Villegas I, Valle Grande B, Bersee H, Benedictus R. A comparative evaluation between flat and traditional energy directors for ultrasonic welding of CF/PPS thermoplastic composites. Compos Interfaces 2015;22(8):717–29.
[16] Villegas I. Strength development versus process data in ultrasonic welding of thermoplastic composites with flat energy directors and its application to the definition of optimum processing parameters. Composites A 2014;65:27–37.
[17] Zhao T, Palardy G, Villegas I, Rans C, Martinez M, Benedictus R. Mechanical behaviour of thermoplastic composites spot-welded and mechanically fastened joints: A preliminary comparison. Composites B 2017;112:224–34.
[18] Villegas I, Rubio P. On avoiding thermal degradation during welding of high-performance thermoplastic composites to thermoset composites. Composites A 2015;77(Supplement C):172–80.
[19] Villegas I, Bersee H. Ultrasonic welding of advanced thermoplastic composites: An investigation on energy-directing surfaces. Adv Polym Technol 2010;29(2):112–21.
[20] Zhao T, Broek C, Palardy G, Villegas I, Benedictus R. Towards robust sequential ultrasonic spot welding of thermoplastic composites: Welding process control strategy for consistent weld quality. Composites A 2018;109:355–67.
[21] Koutras N, Amirdine J, Boyard N, Villegas IF, Benedictus R. Characterisation of crystallinity at the interface of ultrasonically welded carbon fibre PPS joints. Composites A 2019;125:105574.
[22] Tao W, Su X, Wang H, Zhang Z, Li H, Chen J. Influence mechanism of welding time and energy director to the thermoplastic composite joints by ultrasonic welding. J Manuf Processes 2019;37:196–202.
[23] Lessard H, Lebrun G, Benkaddour A, Pham X-T. Influence of process parameters on the thermostamping of a [0/90]12 carbon/polyether ether ketone laminate. Composites A 2015;70:59–68.
[24] Slange T, Warnet L, Grouve W, Akkerman R. Deconsolidation of C/PEEK blanks: on the role of prepreg, blank manufacturing method and conditioning. Composites A 2018;113:189–99.
[25] Ye L, Lu M, Mai Y-W. Thermal de-consolidation of thermoplastic matrix composites - I. Growth of voids. Compos Sci Technol 2002;62(16):2121–30.
[26] Shi H, Villegas IF, Bersee HE. Analysis of void formation in thermoplastic composites during resistance welding. J Thermoplast Compos Mater 2017;30(12):1654–74.
[27] Ye L, Chen Z-R, Lu M, Hou M. De-consolidation and re-consolidation in CF/PPS thermoplastic matrix composites. Composites A 2005;36(7):915–22.
[28] Ogorkiewicz RM, Imperial Chemical Industries, ltd. Plastics Division. Thermoplastics: properties and design. Wiley-interscience publication. London: Wiley; 1974.
[29] Wolfrath J, Michaud V, Månson J-A. Deconsolidation in glass mat thermoplastic composites: Analysis of the mechanisms. Composites A 2005;36(12):1608–16.

[30] Lu M, Ye L, Mai Y-W. Thermal de-consolidation of thermoplastic matrix composites - II. ‘‘migration’’ of voids and ‘‘re-consolidation’’. Compos Sci Technol 2004;64(2):191–202, URL http://www.sciencedirect.com/science/article/pii/S0266353803002331.

[31] Roychowdhury S, Gillespie Jr JW, Advani SG. Volatile-induced void formation in amorphous thermoplastic polymeric materials: I. Modeling and parametric studies. J Compos Mater 2001;35(4):340–66.

[32] Chung JS, Cebe P. Crystallization and melting of cold-crystallized poly(phenylene sulfide). J Polym Sci B: Polym Phys 1992;30(2):163–76.

[33] Furushima Y, Nakada M, Yoshida Y, Okada K. Crystallization/melting kinetics and morphological analysis of polyphenylene sulfide. Macromol Chem Phys 2018;219(2):1700481.

[34] Huo P, Cebe P. Effects of thermal history on the rigid amorphous phase in poly(phenylene sulfide). Colloid Polym Sci 1992;270:840–52.

[35] Belnoue J-H, Nixon-Pearson O, Ivanov D, Hallett S. A novel hyper-viscoelastic model for consolidation of toughened prepregs under processing conditions. Mech Mater 2016;97:118–34.